ZnO Nanowire Arrays on 3D Hierachical Graphene Foam: Biomarker Detection of Parkinson's Disease

Hong Yan Yue,[†,‡,§,#] Shuo Huang,[⊥,#] Jian Chang,[†,‡] Chaejeong Heo,[∥] Fei Yao,[†,‡] Subash Adhikari,[†,‡] Fethullah Gunes,[‡] Li Chun Liu,[‡] Tae Hoon Lee,[†,‡] Eung Seok Oh,[¶] Bing Li,[†,‡] Jian Jiao Zhang,[§] Ta Quang Huy,[†,‡] Nguyen Van Luan,[†,‡] and Young Hee Lee[†,‡,*]

[†]Centre for Integrated Nanostructure Physics, Institute for Basic Science, Sungkyunkwan University, Suwon 440-746, Republic of Korea, [‡]Department of Energy Science, Department of Physics, Sungkyunkwan University, Suwon 440-746, Republic of Korea, [§]School of Materials Science and Engineering, Harbin University of Science and Technology, Harbin 150040, People's Republic of China, [⊥]Department of Neurology, The First Affiliated Hospital of Harbin Medical University, Harbin 150001, People's Republic of China, [∥]Centre for Neuroscience Imaging Research, Institute for Basic Science, Sungkyunkwan University, Suwon 440-746, Republic of Korea, and [¶]Department of Neurology, Chungnam National University Hospital, School of Medicine, Chungnam National University, Daejeon 103-721, Republic of Korea. [#]These authors contributed equally to this work.

ABSTRACT We report that vertically aligned ZnO nanowire arrays (ZnO NWAs) were fabricated on 3D graphene foam (GF) and used to selectively detect uric acid (UA), dopamine (DA), and ascorbic acid (AA) by a differential pulse voltammetry method. The optimized ZnO NWA/GF electrode provided a high surface area and high selectivity with a detection limit of 1 nM for UA and DA. The high selectivity in the oxidation potential was explained by the gap difference between the lowest unoccupied and highest occupied molecular orbitals of a biomolecule for a set of given electrodes. This method was further used to detect UA levels in the serum of patients with Parkinson's disease (PD). The UA level was 25% lower in PD patients than in healthy individuals. This finding strongly implies that UA can be used as a biomarker for PD.

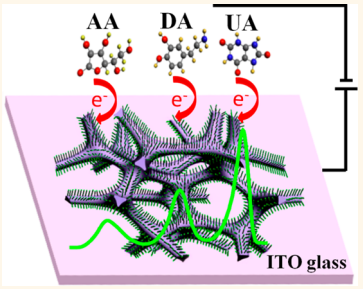

KEYWORDS: ZnO nanowire arrays · graphene foam · biosensor · biomarker detection · Parkinson's disease

Graphene is chemically stable under ambient conditions and has many potential uses in numerous scientific fields and practical applications.[1−3] The use of graphene has been further expanded through integration with other materials for synergistic effects, which often requires tremendous efforts. Recently, graphene foam (GF) consisting of a continuous three-dimensional (3D) interconnected network was used for battery applications.[4,5] GF provides a highly conductive network of defect-free graphene layers without the formation of junction resistance. In addition, GF possesses a high porosity of ~99.7%, which is ideal for use as a scaffold for integration with other materials to generate synergistic effects. In addition, one-dimensional inorganic semiconductor nanowires also represent an attractive class of materials for different sensing applications. Vertically aligned ZnO nanowire arrays (ZnO NWAs) are considered a promising material with high catalytic efficiency, biocompatibility, relative chemical stability in physiological environments, and a large surface area.[6,7] Meanwhile, ZnO NWAs can provide direct and stable pathways for rapid electron transport.[8] The integration of GF and ZnO NWAs with good connectivity can facilitate the use of large area GF with high electrical conductivity to enhance the sensitivity of electrochemical biosensors.

RESULTS AND DISCUSSION

Herein, we report on the hydrothermal synthesis of ZnO NWAs grown on GF using chemical vapor deposition (CVD). A schematic of the fabricated ZnO NWA/GF electrode used to simultaneously detect uric acid (UA), dopamine (DA), and ascorbic acid (AA) is shown in Figure 1a. The ZnO NWAs (shown in olive) were used to cover the surface of the 3D GF (shown in purple). Biomolecules were oxidized to generate protons and electrons during an electrochemical reaction (Supporting Information Figure S1). The generated electrons were quickly transferred to the ZnO NWA/GF electrode.

* Address correspondence to leeyoung@skku.edu.

Received for review November 18, 2013 and accepted January 9, 2014.

Published online January 09, 2014
10.1021/nn405961p

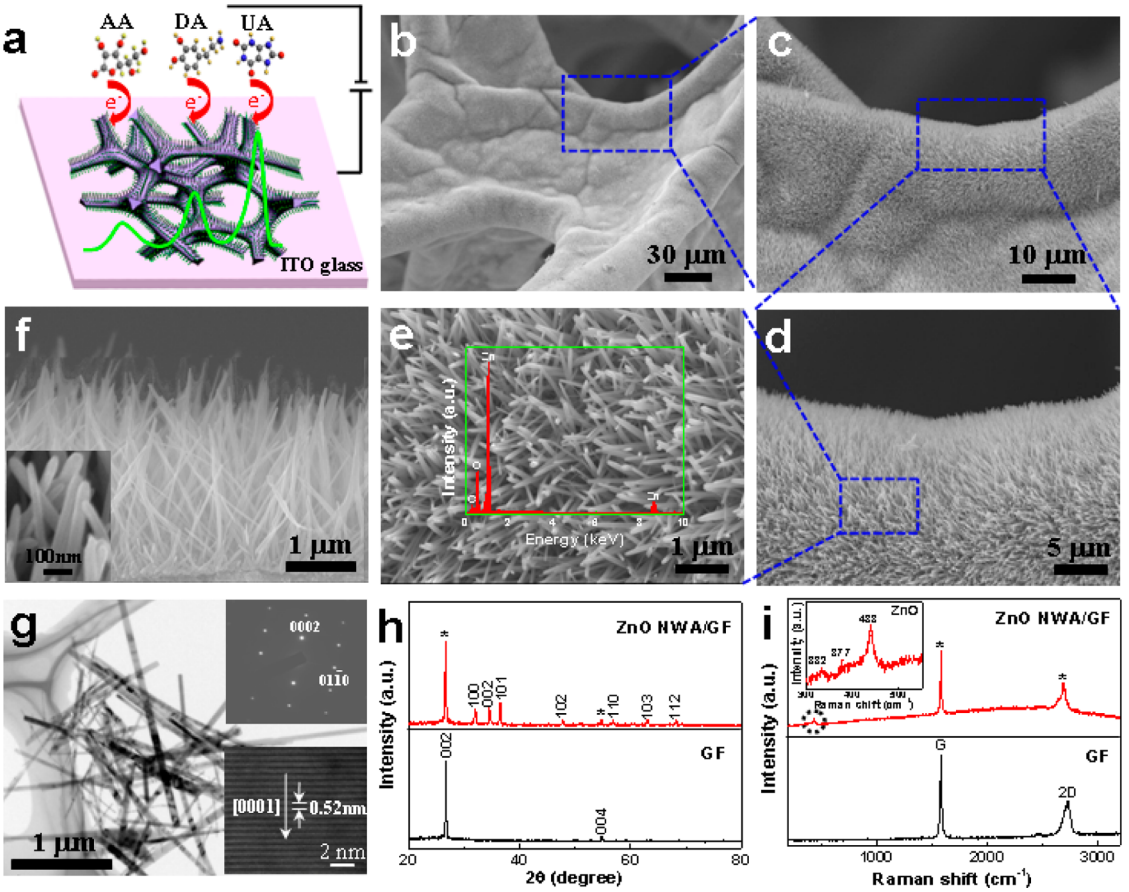

Figure 1. Structural analysis of the integrated ZnO NWA/GF. (a) Schematic of the ZnO NWA/GF electrode and detection of UA, DA, and AA. (b−e) SEM images of the ZnO NWAs on the 3D GF at different magnifications. Inset: EDX of the ZnO NWAs. (f) SEM images of the height of the ZnO NWAs, ∼2 μm. Inset: diameter of the ZnO NWAs, ∼40 nm. (g) TEM images of the ZnO nanowires which were detached from GF by sonication and transferred on the TEM grid. Inset: SAED pattern (top) and HRTEM image of the ZnO nanowire (bottom). (h) XRD patterns and (i) Raman spectra of the GF and ZnO NWA/GF. Inset: magnification of the ZnO NWAs spectrum; "∗"indicates the peaks of the GF.

Figure 1b−f shows a series of scanning electron microscopy (SEM) images of the ZnO NWA/GF structure. GF at the bottom of the ZnO NWAs was robust, and the surface of the GF was fully covered by vertically aligned, highly uniform ZnO NWAs. The ZnO nanowires were ∼40 nm in diameter and 2 μm in height (Figure 1f). During the course of the DPV measurements, the detachment of ZnO NWAs was not observed. ZnO nanowires were then separated from GF by the ultrasonic treatment for TEM image. The ZnO nanowires were single-crystalline with a lattice constant of 0.52 nm, corresponding to the [0001] growth direction, as demonstrated by TEM (Figure 1g). The X-ray diffraction (XRD) pattern of the 3D GF had two significant diffraction peaks at 2θ = 26.5 and 54.6°, which were attributed to the (002) (with an interlayer spacing of 0.34 nm) and (004) reflections of graphite, respectively (JCPDS 75-1621) (bottom of Figure 1h). In the ZnO NWA/GF (top panel), the characteristic diffraction peaks matched well with the standard peak positions for a hexagonal ZnO structure (JCPDS 36-1451) and with the characteristic peaks of GF. The Raman spectrum of the 3D GF contained two prominent peaks near ∼1580 and 2720 cm^{-1}, corresponding to the G and 2D bands of graphene (Figure 1i). No appreciable D band intensity was observed, which confirmed the high quality of the graphene, in contrast to defective reduced graphene oxide.[9] The integrated intensity ratio of the G to 2D band (I_G/I_{2D}) indicates that the as-grown GF was primarily multilayered graphene.[4] In addition to the G and 2D bands for the ZnO NWA/GF, the three peaks shown in the inset near 332, 377, and 438 cm^{-1} are characteristic of the ZnO NWAs (Figure 1i). Therefore, these results confirm the successful integration of the ZnO NWAs and the 3D GF.

Uric acid, which is a primary purine metabolite, is regarded as an important natural antioxidant.[10] Abnormal levels of UA are symptomatic of several diseases, including gout, hyperuricemia, and Parkinson's disease (PD).[11] Dopamine is an important neurotransmitter that is widely distributed within the mammalian central nervous system. Low levels of DA are related to neurological disorders such as PD and schizophrenia.[12] Ascorbic acid is a vital vitamin in the human diet and is well-known for its antioxidant properties.[13] It is also well-known that UA, DA, and AA coexist in the

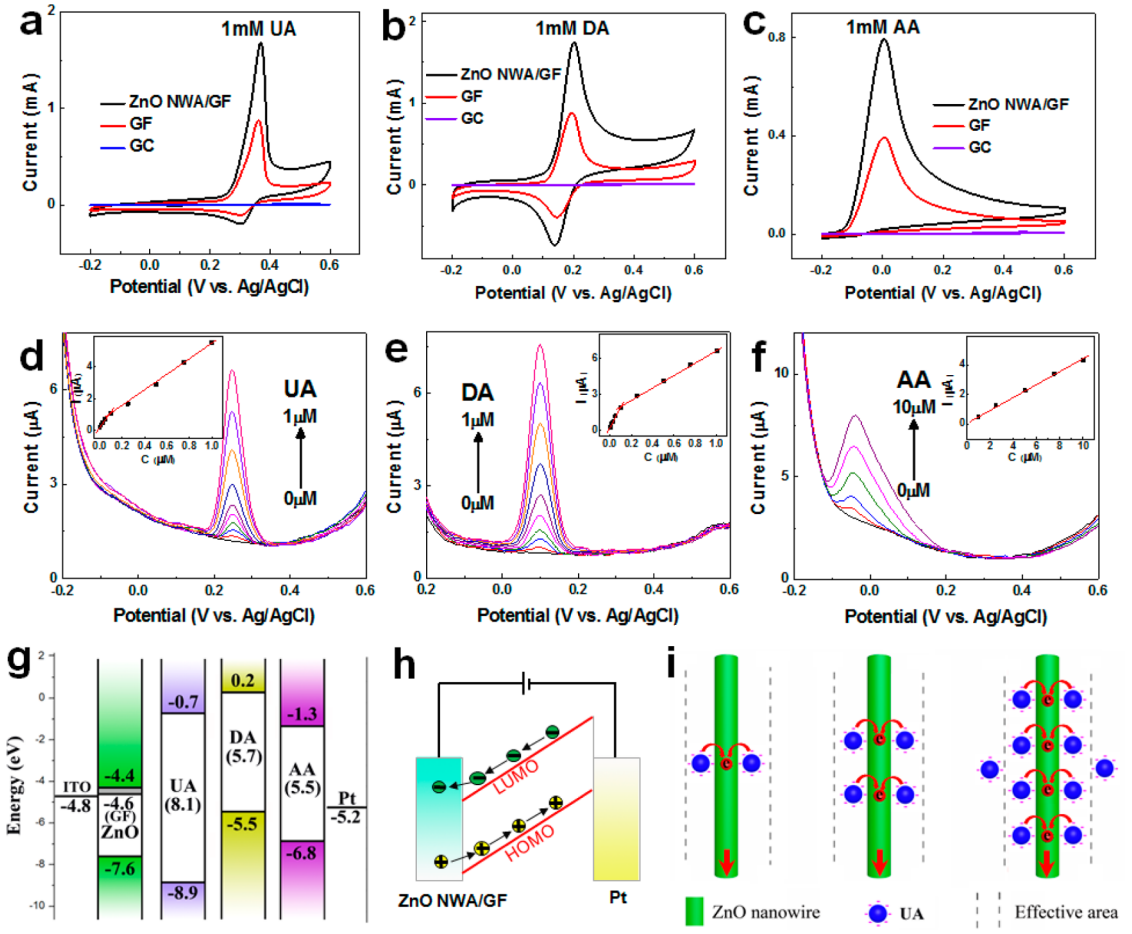

Figure 2. Electrochemical detection of UA, DA, and AA. (a–c) CV curves of the ZnO NWA/GF, GF, and bare GC electrodes in 1 mM UA, DA, and AA, respectively, at a scan rate of 50 mV s^{-1}. (d–f) DPV curves for UA, DA, and AA at different concentrations using a ZnO NWA/GF electrode. The UA concentrations from the bottom are 0, 0.001, 0.01, 0.025, 0.05, 0.1, 0.25, 0.5, 0.75, and 1 μM. The DA concentrations from the bottom are 0, 0.001, 0.01, 0.025, 0.05, 0.1, 0.25, 0.5, 0.75, and 1 μM. The AA concentrations from the bottom are 0, 1, 2.5, 5, 7.5, and 10 μM. Insets: plots of the oxidation peak current *vs* concentration of each biomolecule, showing two slopes for UA and DA. (g) Flat band model (LUMO and HOMO) of the ZnO NWA/GF, UA, DA, and AA, and work function for the GF, ITO, and Pt electrodes. (h) Electron and hole transfer during oxidation of the biomolecules. (i) Schematic of the adsorbed biomolecule (UA) at different concentrations. The supporting electrolyte is a 0.1 M PBS solution (pH 7.4). DPV conditions: a pulse height of 50 mV, a step height of 4 mV, a pulse width of 0.2 s, a step time of 0.5 s, and a scan rate of 8 mV s^{-1}.

extracellular fluid of the central nervous system and serum. However, it is difficult to simultaneously detect each species in a mixture with high selectivity and sensitivity when using conventional solid electrodes[14] because their oxidation potentials overlap, the surface area is insufficient, and/or the kinetic accessibility of each species is limited. Although high-performance liquid chromatography,[15] enzymatic reaction-based spectrophotometric methods,[16] and immunosensing microfluidic systems[17,18] can be used to quantitatively detect these species with a high degree of sensitivity, these approaches are not easily utilized due to high costs from the equipment and disposable chemicals, complicated experimental protocols, and chip structures. Electrochemical methods have attracted attention from a clinical diagnostic perspective due to their simplicity, low cost, high sensitivity and selectivity, excellent reproducibility and stability, and low detection limits.[19,20]

Figure 2a–c shows cyclic voltammetry (CV) curves for various electrodes at a scan rate of 50 mV s^{-1}. The ZnO NWA/GF electrode had the highest oxidation current, with a relatively narrow peak window for the detection of 1 mM UA. The GF is hydrophobic and chemically inert, which impedes electrochemical reactions in an aqueous environment,[21] resulting in a smaller oxidation current compared to that from the ZnO NWA/GF electrode. However, a low oxidation current and broad oxidation peak were observed for the commercial GC electrode (Figure 2a and Supporting Information Figure S9). The oxidation current density of the ZnO NWA/GF electrode was enhanced by a factor of 10 compared to that of the commercial GC electrode. This result may arise from several factors: (i) the central GF provides a pathway for rapid electron transport; (ii) the biomolecules are readily accessible to the 3D hierarchical and porous ZnO NWA/GF surface;

(iii) the ZnO NWAs on the surface of GF offer numerous active sites; and (iv) the ZnO NWA/GF possesses a large surface area (Supporting Information Figure S8). This trend is similar to that observed for DA and AA at the same concentrations but at different oxidation potentials (Figure 2b,c). Moreover, it also suggests a primary diffusion-controlled oxidation process for these biomolecules in a scan range of 10−90 mV s^{-1} (Supporting Information Figure S10). Heat treatment of the ZnO NWA/GF was necessary to obtain distinct oxidation potentials for the UA, DA, and AA (Supporting Information Figures S11−S13), which is again evidence of the increase of active sites in ZnO NWAs after heat treatment. An efficient conductivity of GF and its robust adhesion to ZnO NWAs to facilitate electron conduction were well manifested in the low equivalent series resistance in the impedance measurement (Figure S13).

A differential pulse voltammetry (DPV) method was used to obtain better sensitivity, due to the enhanced analytical signal achieved by eliminating the non-Faradaic current compared to CV.[22] DPV curves for the ZnO NWA/GF electrode at different concentrations of UA, DA, and AA are shown in Figure 2d−f (Supporting Information Figure S14). Four important features that should be noted are as follows: (i) distinct oxidation potentials were observed (UA, 0.25 V; DA, 0.1 V; and AA, −0.04 V); (ii) the oxidation peak currents for UA (5.5 μA) and DA (6.5 μA) were larger than that of AA (0.4 μA) at 1 μM; (iii) the oxidation current increased linearly as the concentration increased, revealing two linear slopes for UA and DA (inset); and (iv) the measured limit of detection (m-LOD) reached 1 nM for UA and DA.

The oxidation potential is generally governed by electron transfer from the biomolecule to the ZnO and hole transfer from the biomolecule to the Pt electrode, although this varies with the electrolyte acidity, scan rate, and biomolecule concentration. The Schottky barrier that forms at the ZnO and biomolecule interface is the main origin of the oxidation potential (Figure 2g). By considering two barriers for the electrons and holes, from a simple flat band model, the oxidation potential is simply determined by the gap between the lowest unoccupied molecular orbital and the highest occupied molecular orbital (LUMO−HOMO) of the biomolecule[23−25] for two given electrodes (Supporting Information Figure S15). UA has the largest LUMO−HOMO gap, resulting in the largest oxidation potential, which agrees with our observations. In addition, the adsorption of biomolecules on the ZnO during oxidation induces a dipole interaction at the interface through the charge transfer, which further modifies the oxidation potential.

The oxidation peak current is determined by the sum of the electron flow to the ZnO and the hole flow to the Pt electrode (Figure 2h). The oxidation current is further modified by the adsorption strength. UA and DA contain an aromatic ring in their molecular structures (Supporting Information Figure S1), resulting in strong adsorption and, hence, high oxidation currents (Figure 2e,f). The m-LOD reached 1 nM for both UA and DA, which is superior to all previously reported limits for individual detection (Supporting Information Table S1). However, the adsorption strength of AA was weak due to the absence of an aromatic ring (Supporting Information Figure S1). As a consequence, the oxidation current was low compared to those of UA and DA, resulting in a relatively poor detection limit.

The existence of two slopes in the oxidation peak current may be explained by monolayer adsorption followed by multilayer adsorption, as shown in the schematic (Figure 2i). Even at low concentrations of UA and DA, the first layer was easily formed due to strong adsorption. In the limit of a high concentration, interactions among the second-layer molecules were screened by the first-layer molecules, which means that the interaction strength differs from that of the first-layer molecules, resulting in two slopes in the peak current. Due to the weak interaction of the AA molecules, multilayer adsorption of the molecules was not realized, even at high concentrations, yielding a single slope. UA and DA had a higher slope than AA, which is reflected as a higher sensitivity.

Due to the coexistence of UA, DA, and AA in numerous biological systems, accurate measurements of each component with a high degree of sensitivity and selectivity are mandatory. Figure 3 depicts DPV curves obtained at various concentrations for each species as the other two species are held at fixed concentrations. For instance, the UA concentration was varied from 0 to 40 μM for fixed concentrations of DA (15 μM) and AA (100 μM) (Figure 3a). The oxidation peak currents for DA and AA remained almost constant as the UA concentration increased. This trend indicates that the addition of UA did not significantly influence the oxidation peak currents or potentials of the other two species. Similar trends were observed for the other species. The m-LODs were 0.5, 0.5, and 5 μM for UA, DA, and AA, respectively, which are much smaller than previously reported values (Supporting Information Table S2). It is possible to simultaneously determine the amount of UA, DA, and AA in a ternary mixture without obvious cross interference. Thus, the ZnO NWA/GF electrode may be a promising candidate for electroanalysis applications due to their improved selectivity and sensitivity and their excellent stability (Supporting Information Figure S16).

To provide a proof of concept, we directly examined serum extracted from human peripheral blood. UA and DA are known biomarkers for PD,[10,26−28] and the facile assessment of PD biomarkers in small volumes of diluted serum is required (see Supporting Information S2 for more details). Figure 4a shows typical DPV curves obtained from PD serum at different concentrations diluted in a 0.1 M PBS solution. A small broad peak at −0.02 V and two obvious peaks at 0.15 and 0.29 V

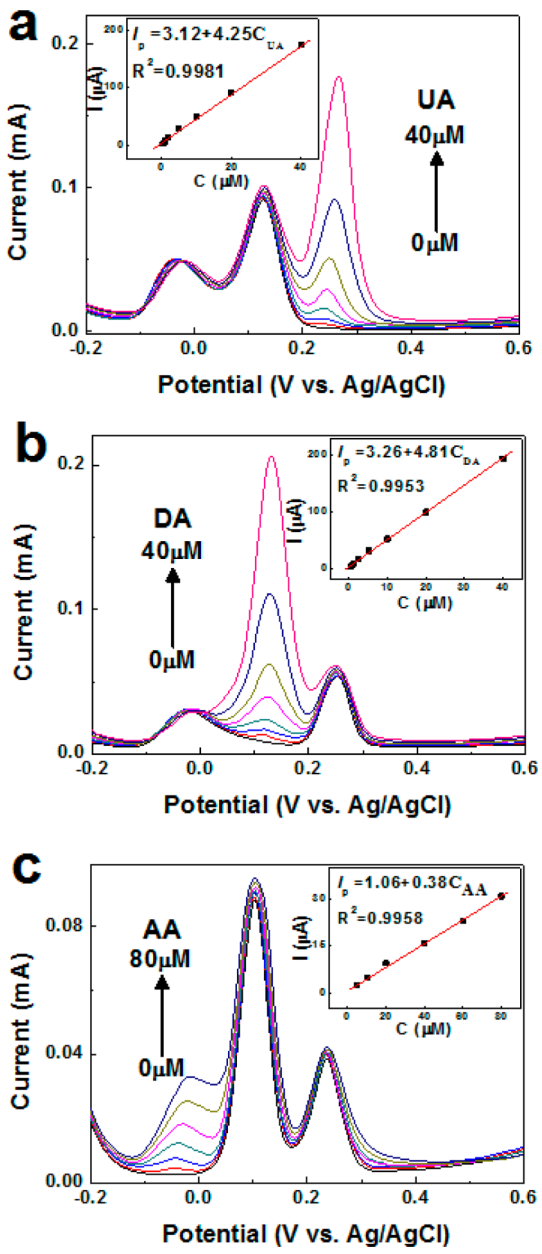

Figure 3. DPV measurements for mixed UA, DA, and AA. DPV curves for the ZnO NWA/GF electrode at varying concentrations of (a) UA in a mixture of 100 μM AA and 15 μM DA; the UA concentrations from the bottom are 0, 0.5, 1, 2.5, 5, 10, 20, and 40 μM; (b) DA in a mixture of 50 μM AA and 10 μM UA; the DA concentrations from the bottom are 0, 0.5, 1, 2.5, 5, 10, 20, and 40 μM; (c) AA in a mixture of 15 μM DA and 7.5 μM UA; AA concentrations from the bottom are 0, 5, 10, 20, 40, 60, and 80 μM. Insets: plots of the oxidation peak current *vs* the concentration of each biomolecule. The supporting electrolyte and the DPV conditions are the same as in Figure 2.

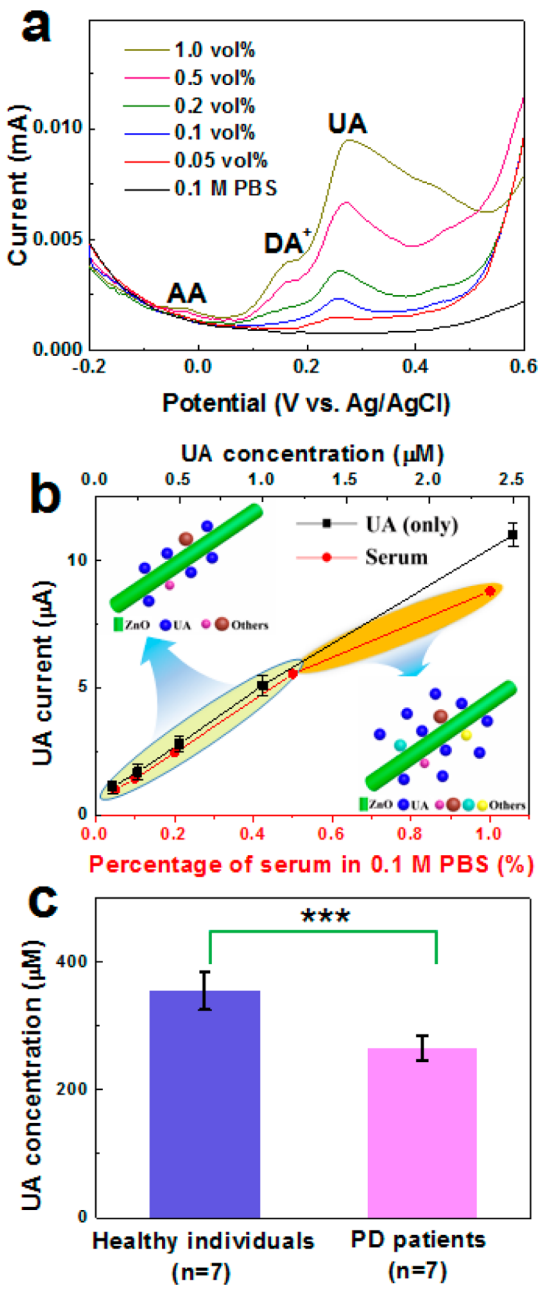

Figure 4. DPV measurements in serum of patients from Parkinson's disease (PD). (a) DPV curves of different volume fractions of PD serum in a 0.1 M PBS solution (pH 7.4) for a ZnO NWA/GF electrode. (b) Relationship between the UA peak current and the percentage of serum in a 0.1 M PBS solution (the calibration curve is shown in black). The error bars represent the standard deviation obtained from four measurements. (c) Statistical analysis of healthy individuals and PD patients serum UA levels in a 0.1 M PBS solution. The average serum UA levels were 355 $\pm$ 30 μM in the healthy individuals (n = 7) and 265 $\pm$ 20 μM in the PD patients (n = 7), respectively. Inset: asterisks denoted data points representing an experimental group significantly different statistically (***p < 0.001) from healthy control group. The DPV conditions are the same as in Figure 2.

were observed when a 0.2 vol % serum or greater is used. The potential near −0.02 V corresponds to AA oxidation. The peak near 0.15 V corresponds to DA oxidation but overlaps with signals from norepinephrine, epinephrine, and L-dopa,[29] excluding the possibility of its use as a biomarker for PD. The peak near 0.29 V originates from the UA. The relationship between the UA peak current and the percentage of serum in a 0.1 M PBS solution is shown in Figure 4b. The oxidation current level of the UA from the serum was similar to that of the UA solution as the percentage of serum increased, but the slope decreased over 0.5% (equivalently 1.25 μM UA). At serum

concentrations below 0.5%, the UA can be effectively adsorbed on the ZnO surface and reacted directly, leaving no appreciable change in the oxidation current compared with the UA solution only. At concentrations greater than 0.5%, other species are involved in the adsorption with UA (see the schematic in the inset). To determine accurate UA levels in PD patients, the serum was diluted 500-fold using a 0.1 M PBS solution. Assays were run on samples from seven healthy individuals and seven PD patients. The average UA concentrations for the healthy individuals and the PD patients were 355 ± 30 and 265 ± 20 μM, respectively (Figure 4c and Supporting Information Figure S17). This clear reduction in UA levels in the serum of PD patients with reliable statistics ($p < 0.001$) strongly implies that our approach is a significant step forward, which we believe will be beneficial for diagnosising PD and monitoring disease progression.

CONCLUSIONS

We have fabricated vertically aligned ZnO nanowire arrays on 3D graphene foam which were used to selectively detect UA, DA, and AA by a differential pulse voltammetry method. The key features for the structural design were large surface area with mesoporous 3D graphene structures to facilitate ion diffusion easily, high conductivity from 3D graphene foam, and active sites of ZnO surface for high selectivity. The thermal annealing was necessary to manifest selectivity on the ZnO surface among UA, DA, and AA. The optimized ZnO NWA/GF electrode provided high selectivity with a detection limit of 1 nM for UA and DA. The selectivity in the oxidation potential was explained by the gap difference between the lowest unoccupied and highest occupied molecular orbitals of a biomolecule for a set of given electrodes. For field test of Parkinson's disease, the UA level was 25% lower within reliable statistical statistics in PD patients than in healthy individuals. This finding opens a possibility that UA can be used as a biomarker for PD, which will provide greater clinical diagnostic power and the potential to improve disease prognoses.

METHODS

Summary. Nickel foams were used as 3D templates for the growth of GF by atmospheric pressure chemical vapor deposition (APCVD). After etching the nickel, the obtained GF was transferred onto ITO glass. A solution of 0.01 M $Zn(CH_3COO)_2 \cdot 2H_2O$ in methanol was then dropped on the surface of the GF to prepare for the ZnO seeding layer. The ZnO-seeded GF on the ITO glass was placed top-down and was immersed in a mixture of $Zn(NO_3)_2 \cdot 6H_2O$ (0.05 M), hexamethylenetetramine (HMTA, 0.05 M), $NH_3 \cdot H_2O$ (0.05 M), and polyethylenimine (PEI, 2 mM) to prepare the ZnO NWA/GF under hydrothermal conditions at 100 °C for 12 h. Finally, the ZnO NWA/GF was rinsed in deionized water and annealed in air at 450 °C for 1 h. The CV and DPV methods were used to measure the current response of the UA, DA, and AA biomolecules at different concentrations. The application of this ZnO NWA/GF electrode was evaluated by assaying the UA levels of clinical serum samples from healthy individuals and PD patients using the DPV method.

Reagents and Chemicals. All reagents and chemicals were analytical grade, purchased from Sigma-Aldrich, and were directly used for the following experiments. Deionized water with a resistivity greater than 18.0 MΩ was used in all of the assays and solutions. UA, DA hydrochloride, and AA solutions were prepared daily and stored in a refrigerator.

Synthesis of 3D GF. Nickel foams (Alantum Advanced Technology Materials, China) with an areal density of 420 g m^{-2} and a thickness of 1.6 mm were used as 3D templates for the growth of GF by atmospheric pressure chemical vapor deposition (APCVD) (Supporting Information Figures S2 and S3). Nickel foams were placed in the center of a quartz tube in an APCVD chamber, and samples were heated to 1000 °C at a rate of 30 °C min^{-1} in an Ar (500 sccm) and H_2 (200 sccm) flow. The temperature was maintained for 30 min to reduce the formation of oxides on the surface of the nickel foams. A CH_4 gas (20 sccm) was then flowed for 10 min with the same amounts of Ar and H_2. Following the synthesis, the CH_4 gas was turned off and the chamber was cooled to room temperature at a rate of 100 °C min^{-1}. The resulting samples were cut into 1 × 1 cm^2 pieces, and the nickel foams were covered with graphene drop-coated with a poly(methyl methacrylate) (PMMA) solution (molecular weight ≈ 996 000, 4 wt % PMMA in ethyl lactate) and baked at 180 °C for 30 min. This process is necessary to retain the porous structures. The sample was then placed in a nickel etchant (Transene Inc., TFB) at 90 °C for 5 h to completely remove the nickel. Finally, free-standing GF was obtained by dissolving the PMMA with hot acetone at 60 °C for 1 h. After etching the nickel, the obtained GF was transferred onto the ITO glass (specific resistance of <10 Ω, Zhuhai Kaivo Electronic Co., Ltd., China), which acts as an electrode. The ITO glass was sonically cleaned in an acetone/ethanol solution prior to use.

Synthesis of ZnO NWA/GF. The hydrothermal synthesis method for preparing ZnO NWAs is more favorable for practical applications due to its low growth temperature, low cost, and potential for scale-up.[30] Here, we expand on this method to produce the homogeneous vertical ZnO NWAs on the surface of the prepared GF under mild aqueous conditions. The GF was transferred onto ITO glass to prepare the ZnO NWA/GF under hydrothermal conditions. Initially, 0.01 M $Zn(CH_3COO)_2 \cdot 2H_2O$ was dispersed in methanol. The solution was dropped onto the surface of the GF and was annealed at 200 °C to form a seeding layer of ZnO nanocrystals. A mixed solution consisting of $Zn(NO_3)_2 \cdot 6H_2O$ (0.05 M), hexamethylenetetramine (HMTA, 0.05 M), $NH_3 \cdot H_2O$ (0.05 M), and PEI (2 mM) was prepared. After stirring for 5 min under ambient conditions, the mixture was transferred to a Teflon-lined stainless steel autoclave with a volume of 100 mL. The ZnO-seeded GF was fixed onto the ITO glass, placed top-down, and immersed in the mixture solution. A hydrothermal treatment was conducted at 100 °C for 12 h. Afterward, the autoclave was allowed to cool to ambient temperature. The effect of the preparation parameters on the morphology and cross section of the ZnO NWA/GF was also investigated (Supporting Information Figures S4–S7). Finally, the ZnO NWA/GF was rinsed with deionized water and annealed in air at 450 °C for 1 h to remove any residual organics.

Scanning Electron Microscopy (SEM). A field-emission scanning electron microscope (FE-SEM; JSM7600F, JEOL) equipped with an energy-dispersive spectrometer (EDAX) operating at an acceleration voltage of 20 kV was used to examine the surface morphology and to conduct elemental analysis of the samples.

Transmission Electron Microscopy (TEM). A high-resolution transmission electron microscope (HRTEM; JEM2100F, JEOL) was used to investigate the morphologies of the GF and the ZnO nanowires and the electron diffraction patterns of the ZnO nanowires. An accelerating voltage of 200 kV was used. For the TEM observations, the ZnO NWA/GF was ultrasonically dispersed in ethanol for 3 min, and the detached ZnO nanowires

from GF were dropped onto a 200-mesh TEM grid, followed by drying under ambient conditions.

X-ray Diffraction (XRD) and Raman Spectroscopy. The crystallographic structures of the GF and ZnO NWA/GF were directly examined by using XRD (Rotaflex D/MAX System, Rigaku) with Cu Kα radiation (λ = 0.15406 nm). Raman spectroscopy was performed with a micro-Raman system (Renishaw, RM1000-In Via) using an excitation energy of 1.96 eV (633 nm, HeNe laser).

Brunauer–Emmett–Teller (BET) Measurement. The specific surface area was determined by measuring N_2 adsorption–desorption isotherms at 77 K using a Quantachrome ASAP2020. The micropore and mesopore size distributions were calculated by the Horvath–Kawazoe (HK) and Barrett–Joyner–Halenda (BJH) methods, respectively.

Thermogravimetric Analysis (TGA). A TGA (Q500, TA Instrument) was used to determine the heat treatment temperature of the ZnO NWA/GF. The temperature was increased at a rate of 5 °C min^{-1} in an air atmosphere from room temperature to 500 °C.

Sheet Resistance Measurements. The sheet resistance of the GF and ZnO NWA/GF (before and after heat treatment) on glass was measured using a four-point method with a Keithley 2000 multimeter at room temperature.

Electrochemical Measurements. All of the electrochemical measurements, including CV, DPV, and electrochemical impedance spectroscopy (EIS), were performed in a 0.1 M PBS solution (pH 7.4) using a VMP3 electrochemical workstation (BioLogic Science Instrument, France) in a three-electrode cell at room temperature (Supporting Information Figure S18). The free-standing ZnO NWA/GF electrode served as the working electrode, a Ag/AgCl electrode as the reference electrode, and a platinum wire as the counter electrode. The apparent area of the ZnO NWA/GF electrode was 0.7 cm^2. CV experiments were carried out at a scan rate of 50 mV s^{-1} unless otherwise stated. The DPV responses were recorded over a potential range of −0.2 to 0.6 V with the following parameters: a pulse height of 50 mV, a step height of 4 mV, a pulse width of 0.2 s, a step time of 0.5 s, and a scan rate of 8 mV s^{-1} (Supporting Information Figure S19). The EIS was measured over a frequency range of 100 kHz to 10 MHz at the open-circuit potential and with a perturbation signal of 10 mV.

Human Serum. Seven PD patients (4 males and 3 females) aged 66.6 ± 9.8 years were recruited from the outpatient clinic of the Department of Neurology at the Chungnam National University Hospital. The patients were neurologically examined to confirm the presence of clinically definite PD according to the clinical criteria of the UK PD Society Brain Bank.[17] Data regarding age, gender, disease duration, and pharmacological treatment were obtained for each participating patient. Patients with concomitant neurological or psychiatric diseases, cancer, or other severe diseases were excluded. Seven healthy individuals (5 males and 2 females) aged 63.8 ± 8.9 years and biologically unrelated to the PD patients were selected as controls. The exclusion criteria for the control individuals were identical to those of the PD patients. All participants gave their written informed consent after receiving information on the details of the study according to the *Declaration of Helsinki ethical guidelines*. The study protocol was approved by the scientific ethics committee of the Chungnam National University Hospital.

Statistical Analysis. The bar graph of serum UA levels from human peripheral blood was shown as average value with a standard deviation. An independent two-sample *t* test (SPSS 19, International Business Machines Corp., NY, USA) was performed to evaluate statistical differences. Asterisks *** denoted data representing an experimental group significantly different statistically ($p < 0.001$) between healthy individuals control and PD patients.

Conflict of Interest: The authors declare no competing financial interest.

Acknowledgment. This work was supported by the Institute for Basic Science (IBS), the World Class University (WCU) program (2008-000-10029-0) of the National Research Foundation of Korea (NRF) funded by the Ministry of Education, Science and Technology (MEST) of Korea. H.Y.Y. acknowledges the financial support from Natural Science Research Foundation of China (No. 51201052) and Science Funds for the Young Innovative Talents of HUST (No. 201306), and S.H. acknowledges the financial support from postdoctoral science foundation of Heilongjiang province (LBH-Z11064) and China (2013M541412).

Supporting Information Available: Materials and methods, supplementary text, Figures S1–S19, Table S1 and S2, and references. This material is available free of charge *via* the Internet at http://pubs.acs.org.

REFERENCES AND NOTES

1. Novoselov, K. S.; Fal'ko, V. I.; Clombo, L.; Gellert, P. R.; Schwab, M. G.; Kim, K. A Roadmap for Graphene. *Nature* **2012**, *490*, 192–200.
2. Chen, S.; Brown, L.; Levendorf, M.; Cai, W.; Ju, S. Y.; Edgeworth, J.; Li, X.; Magnuson, C. W.; Velamakanni, A.; Piner, R. D.; *et al.* Oxidation Resistance of Graphene-Coated Cu and Cu/Ni Alloy. *ACS Nano* **2011**, *5*, 1321–1327.
3. Liu, Y.; Dong, X.; Chen, P. Biological and Chemical Sensors Based on Graphene Materials. *Chem. Soc. Rev.* **2012**, *41*, 2283–2307.
4. Chen, Z.; Ren, W.; Gao, L.; Liu, B.; Pei, S.; Cheng, H. M. Three-Dimentional Flexible and Conductive Interconnected Graphene Networks Grown by Chemical Vapour Deposition. *Nat. Mater.* **2011**, *10*, 424–428.
5. Li, N.; Chen, Z.; Ren, W.; Li, F.; Cheng, H. M. Flexible Graphene-Based Lithium Ion Batteries with Ultrafast Charge and Discharge Rates. *Proc. Natl. Acad. Sci. U.S.A.* **2012**, *109*, 17360–17365.
6. Kenry; Lim, C. T. Synthesis, Optical Properties, and Chemical-Biological Sensing Applications of One-Dimensional Inorganic Semiconductor Nanowires. *Prog. Mater. Sci.* **2013**, *58*, 705–748.
7. Wang, Z. L.; Song, J. H. Piezoelectric Nanogenerators Based on Zinc Oxide Nanowire Arrays. *Science* **2006**, *312*, 242–246.
8. Law, M.; Greene, L. E.; Johnson, J. C.; Saykally, R.; Yang, P. Nanowire Dye-Sensitized Solar Cells. *Nat. Mater.* **2005**, *4*, 455–459.
9. Yoon, S. M.; Choi, W. M.; Baik, H.; Shin, H. J.; Song, I.; Kwon, M. S.; Bae, J. J.; Kim, H.; Lee, Y. H.; Choi, J. Y. Synthesis of Multilayer Graphene Balls by Carbon Segregation from Nickel Nanoparticles. *ACS Nano* **2012**, *6*, 6803–6811.
10. Hass, B. R.; Stewart, T. H.; Zhang, J. Premotor Biomarkers for Parkinson's Disease: A Promising Direction of Research. *Transl. Neurodegener.* **2012**, *1*, 11.
11. Sheng, Z. H.; Zheng, X. Q.; Xu, J. Y.; Bao, W. J.; Wang, F. B.; Xia, X. H. Electrochemical Sensor Based on Nitrogen Doped Graphene: Simultaneous Determination of Ascorbic, Dopamine and Uric Acid. *Biosens. Bioelectron.* **2012**, *34*, 125–131.
12. Sun, C. L.; Chang, C. T.; Lee, H. H.; Zhou, J.; Wang, J.; Sham, T. K.; Pong, W. F. Microwave-Assisted Synthesis of a Core–Shell MWCNT/GONR Heterostructure for the Electrochemical Detection of Ascorbic Acid, Dopamine, and Uric Acid. *ACS Nano* **2011**, *5*, 7788–7795.
13. Thompson, J.; Manore, M.; Vaughan, L. *The Science of Nutrition*, 3rd ed.; Benjamin Cummings: San Francisco, CA, 2013; Chapter 10.
14. Sekli-Belaidi, F.; Temple-Boyer, P.; Gros, P. Voltammetric Microsensor using PEDOT-Modified Gold Electrode for the Simultaneous Assay of Ascorbic and Uric Acids. *J. Electroanal. Chem.* **2010**, *647*, 159–168.
15. Wu, L.; Feng, L.; Ren, J.; Qu, X. Electrochemical Detection of Dopamine Using Porphyrin-Functionalized Graphene. *Biosens. Bioelectron.* **2012**, *34*, 57–62.
16. Gochman, N.; Schmitz, J M. Automated Determination of Uric Acid, with Use of a Uricase-Peroxidase System. *Clin. Chem.* **1971**, *17*, 1154–1159.
17. Yu, J.; Ge, L.; Huang, J.; Wang, S.; Ge, S. Microfluidic Paper-Based Chemiluminescence Biosensor for Simultaneous Determination of Glucose and Uric Acid. *Lab Chip* **2011**, *11*, 1286–1291.
18. Sansuk, S.; Bitziou, E.; Joseph, M. B.; Covington, J. A.; Boutelle, M. G.; Unwin, P. R.; Macpherson, J. V. Ultrasensitive Detection of Dopamine Using a Carbon Nanotube Network Microfluidic Flow Electrode. *Anal. Chem.* **2013**, *85*, 163–169.

19. Bryan, T.; Luo, X.; Forsgren, L.; Morozova-Roche, L. A.; Davis, J. J. The Robust Electrochemical Detection of a Parkinson's Disease Marker in Whole Blood Sera. *Chem. Sci.* **2012**, *3*, 3468–3473.
20. Lang, X. Y.; Fu, H. Y.; Hou, C.; Han, G. F.; Yang, P.; Liu, Y. B.; Jiang, Q. Nanoporous Gold Supported Cobalt Oxide Microelectrodes as High-Performance Electrochemical Biosensors. *Nat. Commun.* **2013**, *4*, 2169.
21. Chen, Q.; Huang, H.; Chen, W.; Wee, A. T.; Feng, Y. P.; Chai, J. W.; Zhang, Z.; Pan, J. S.; Wang, S. J. *In Situ* Photoemission Spectroscopy Study on Formation of HfO_2 Dielectrics on Epitaxial Graphene on SiC Substrate. *Appl. Phys. Lett.* **2010**, *96*, 07211.
22. Hadi, M.; Rouhollahi, A. Simultaneous Electrochemical Sensing of Ascorbic Acid, Dopamine and Uric Acid at Anodized Nanocrystalline Graphite-like Pyrolytic Carbon Film Electrode. *Anal. Chim. Acta* **2012**, *721*, 55–60.
23. Yadav, R. A.; Rani, P.; Kumar, M.; Singh, R.; Singh, R.; Singh, N. P. Experimental IR and Raman Spectra and Quantum Chemical Studies of Molecular Structures, Conformers and Vibrational Characteristics of L-Ascorbic Acid and its Anion and Cation. *Spectrochim. Acta* **2011**, *84*, 6–21.
24. Mohammad-Shiri, M.; Ghaemi, M.; Riahi, S.; Akbari-Sehat, A. Computational and Electrochemical Studies on the Redox Reaction of Dopamine in Aqueous Solution. *Int. J. Electrochem. Sci.* **2011**, *6*, 317–336.
25. Masoud, M. S.; Ali, A. E.; Shaker, M. A.; Elasala, G. S. Synthesis, Computational, Spectroscopic, Thermal and Antimicrobial Activity Studies on Some Metal-Urate Complexes. *Spectrochim. Acta, Part A* **2012**, *90*, 93–108.
26. Cipriani, S.; Chen, X.; Schwarzschild, M. A. Urate: A Novel Biomarker of Parkinson's Disease Risk, Diagnosis and Prognosis. *Biomarkers Med.* **2010**, *4*, 701–712.
27. Schwarzschild, M. A.; Schwid, S. R.; Marek, K.; Watts, A.; Lang, A. E.; Oakes, D.; Shoulson, I.; Ascherio, A. Parkinson Study Group PRECEPT Investigators, Hyson, C.; Gorbold, E.; *et al*. Serum Urate as a Predictor of Clinical and Radiographic Progression in Parkinson Disease. *Arch. Neurol.* **2008**, *65*, 716–723.
28. Kish, S. J.; Shannak, K.; Hornykiewicz, O. Uneven Pattern of Dopamine Loss in the Striatum of Patients with Idiopathic Parkinson's Disease. Pathophysiologic and Clinical Implications. *N. Engl. J. Med.* **1988**, *318*, 876–880.
29. Atta, N. F.; El-Kady, M. F.; Galal, A. Simultaneous Determination of Catecholamines, Uric Acid and Ascorbic Acid at Physiological Levels Using Poly(*N*-methylpyrrole)/Pd-Nanoclusters Sensor. *Anal. Biochem.* **2010**, *400*, 78–88.
30. Park, H.; Chang, S.; Jean, J.; Cheng, J. J.; Araujo, P. T.; Wang, M.; Bawendi, M. G.; Dresselhaus, M. S.; Bulović, V.; Kong, J.; *et al*. Graphene Cathode-Based ZnO Nanowire Hybrid Solar Cells. *Nano Lett.* **2013**, *13*, 233–239.